Journal of Cleaner Production 262 (2020) 121209

Contents lists available at ScienceDirect

Journal of Cleaner Production

journal homepage: www.elsevier.com/locate/jclepro

Understanding room-temperature magnetic properties of anthropogenic ashes from municipal solid waste incineration to assess potential impacts and resources

V. Funari [a, *], L. Mantovani [b], L. Vigliotti [a], E. Dinelli [c], M. Tribaudino [b]

[a] Dipartimento di Scienze del Sistema Terra e Tecnologie per l'Ambiente, Consiglio Nazionale delle Ricerche, ISMAR-CNR, Bologna, Italy
[b] Dipartimento di Scienze Chimiche, della Vita e della Sostenibilità Ambientale, Università degli Studi di Parma, Parma, Italy
[c] Dipartimento di Scienze Biologiche Geologiche e Ambientali, Alma Mater Studiorum - Università di Bologna, Bologna, Italy

ARTICLE INFO

Article history:
Received 30 April 2019
Received in revised form
7 February 2020
Accepted 18 March 2020
Available online 28 March 2020

Handling editor: Gang Liu

Keywords:
Municipal solid waste incineration (MSWI)
Fly ash and bottom ash
Iron oxides
Superparamagnetic (SP) particles
Anthropogenic pollution

ABSTRACT

Environmental magnetic studies are widely used to trace sources of anthropogenic pollution and have revealed promising applications to the urban waste management system. Here, a collection of solid samples from Municipal Solid Waste Incinerators (MSWI) were studied to probe the capability of geochemical and magnetic data integration as a tool for assessing mineralogy, grain-size, and metal enrichment. A data set of room-temperature magnetic parameters was compared with chemical data by X-ray fluorescence and electron microscopy observations. The aim was to validate or reject methods for urban mining purposes, testing and exploiting the correlations that magnetic properties typically experience with iron and heavy metals, as well as their relation to magnetic grain-sizes (from mm-scale down below 30 nm). We noted that the room-temperature magnetic data of MSWI ashes, used to assess grain-size according to the magnetic domain states, is complicated by the clumping of tiny and large grains displaying similar magnetic properties, so it needs to be supported by optical methods or more advanced magnetic techniques. On the other hand, the integration between magnetic and geochemical data, constrained by the analyses of the magnetic/diamagnetic extracts, helped in assessing magnetic mineral assemblages and potential metal enrichment.

1. Introduction

In the present context of high metals-demand, Europe is confronted with many challenges that are reshaping the anthropogenic resource management system of most raw materials value chains. Such a process has begun at the exploration level to secure stable and sustainable access to raw materials and ends downstream of the production chains, i.e., to the waste treatment and material recycling, in order to efficiently close the loop of a circular economy. The pressing need of raw materials, especially those minerals and metals regarded as "critical" for the EU (European Commission, 2014), means either mining deeper the primary mineral resources or using new types of ores such as waste stocks and flows (Fellner et al., 2015). Being the latter a compelling option for sustainable development, the concept of urban mining sprouted leading to an increased awareness of potentially mineable urban ores. At present, anthropogenic materials such as Municipal Solid Waste Incineration (MSWI) residues are diagnosed for environmental purposes or quality assessment for afteruse using a wide range of methods (Quina et al., 2018).

According to EU Directive 2000/76/EC3, the level of harmfulness and total quantities of incinerated waste must be minimised, and the final solid residue should be recycled where appropriate. In Italy, from 2013 to 2017, the total amount of municipal waste sent to incinerators averaged 6.11 Mt/a, leading to the production of 1.4 Mt/a combustion residues (ISPRA, 2018) called bottom ash (BA) and fly ash (FA). The BA is a non-combustible residue that remains at the bottom of incineration grate furnace; FA comprises the fine particles that rise during combustion and are recovered in secondary steps via air pollution control system. Combustion generally means increased concern of the air pollution adverse effects on the environment and human health since thermally-generated pollutants are as fine or ultrafine as to enter the most vulnerable ecosystem

* Corresponding author. Consiglio Nazionale delle Ricerche, Dipartimento di Scienze Del Sistema Terra e Tecnologie per l'Ambiente, ISMAR-CNR u.o.s. Bologna, Via Gobetti, 101 – 40129, Bologna, Italy.
E-mail address: valerio.funari@bo.ismar.cnr.it (V. Funari).

https://doi.org/10.1016/j.jclepro.2020.121209
0959-6526/

sinks (Englert, 2004).

As a consequence, systematic studies on anthropogenic spots of pollution (Hoesly et al., 2018) are being undertaken with particular focus on MSWI systems (Bayuseno and Schmahl, 2010; Brännvall and Kumpiene, 2016; Eusden et al., 1999; Funari et al., 2016a) to prompt relevant work practices and directives not only on waste recycling but also on emission reduction (Maas and Grennfelt, 2016). It has been recognised that iron is the most abundant component in the finest filterable particulate matter (Wang et al., 2018) and that, in connection with anthropogenic sources, combustion produces magnetic nanoparticles in the form of loose spherules and aggregates (Funari et al., 2018). Thereby, environmental magnetic studies are offering unique pathways to explore the magnetic behaviour of Fe-bearing minerals when combined to geochemical data (Li et al., 2017; Moskowitz et al., 2015; Oldfield, 1991; Rachwał et al., 2017), and they are also getting renewed importance in compliance with the integrated approach invoked by the United Nations Economic Commission for Europe (UNECE) (Maas and Grennfelt, 2016).

Magnetic properties reflect fundamentally different magnetization mechanisms. For example, superparamagnetic (SP) and multi-domain (MD) particles have some similarities in their magnetic response that however differs from the single-domain (SD) grains. In parallel, some grains exhibit transitional and mixed behaviours between those of true MD and SD grains, termed pseudo single-domain (PSD), to which most anthropogenic materials ought to belong (e.g., Magiera et al., 2011). This uncertainty is likely tied to the fact that the theory of magnetic state domains in the PSD range is still debated, but also it highlights the lack of comprehensive and structured dataset for anthropogenic materials. Traditionally, magnetic state domains can be referred to specific grain-size ranges theoretically determined for pure magnetites (SP < 30 nm; 30 nm < SD < 84 nm; 84 nm < PSD< 17 μm; MD > μ17 m) (Moskowitz et al., 2015), but the environmental and industrial processes that dictate the presence of coarse versus fine magnetic grains are affected by a large number of variables in real-world situations that prevents from firm conclusions. However, several environmental magnetic studies linked magnetic properties to the occurrence of metals in soils contaminated by industrial activities (Rachwał et al., 2017; Zhang et al., 2011). Heavy metals and other elements sensitive to substitution into vacancy defects do form bonding with ferrous materials; these elements are incorporated in the ferro(i)magnetic mineral lattice during combustion process or they get adsorbed on the surface of ferro(i)magnetic materials already existing (Chaparro et al., 2004). A literature search revealed numerous studies on the correlation between magnetic data and chemical composition. In soils, magnetic data well correlate with Cr, Sr, Fe, Cu, Mn, Pb, Zn, and Ni (Rachwał et al., 2017; Reyes et al., 2011). The concentration of Fe, Mn, Pb, Zn, and Ni were reported in good association with magnetic susceptibility for anthropogenic materials such as metallurgical dust and fly ashes (Magiera et al., 2011; Szuszkiewicz et al., 2015). Magnetic susceptibility measurements have also been used as a tool to map areas with higher heavy metals contents and to study the lithological and pedological impact on magnetic susceptibility [e.g., Jakšík et al., 2016].

The need for a breakthrough in the waste management system gives improved confidence to undertake magnetic monitoring of anthropogenic materials via a bottom-up approach that combines data from targeted waste categories aimed at defining the potential of magnetic properties for more accurate screening of anthropogenic materials. To span the range of analytical observation and take different approaches into account in the urban waste management, we aim to encourage room temperature magnetic measurements by providing an integrated environmental magnetic study on a collection of BA and FA from Italian MSWI plants. It is quite conceivable that sustainable mining from MSWI waste materials could become unattainable simply due to low concentrations of ore metals and heterogeneous composition of the starting waste materials (Funari et al., 2015; Quina et al., 2018). Nevertheless, it would be crucially important to be able to clearly distinguish the finest magnetic grain size and getting rapid information about metal contents in anthropogenic materials for prospecting and monitoring purposes. Efficient urban mining is economically viable when operating at a certain size and with sufficient predictability assessed in the smaller scales, so it relies on fine-tuned techniques to prospect, upgrade, and extract the required raw material and, in parallel, to advance in environmental protection and assessment of critical raw materials from atypical ores.

2. Materials and methods

2.1. Collection of MSWI samples

A collection of BA and FA samples was taken from four Italian MSWI systems following the sampling methodology as in Funari et al., (2015). The selected facilities are located in four different municipalities and serve an area of about 10,000 km^2 within the Po Valley, the most densely populated area of northern Italy. Each incinerator, equipped with a grate-furnace system, operates at temperatures between 850 and 1100 °C. The solid waste input, which averages $1.5 \cdot 10^5$ t/a, consists of 90% household waste and 10% of special waste. The fraction of special waste includes scraps from ceramics, processing waste from steel-making industries, automobile shredder residues, and hospital/pharmaceutical waste, being the latter the smallest fraction. The solid waste output averages $4.6 \cdot 10^4$ t/a BA and $4.1 \cdot 10^3$ t/a FA, respectively. The figure for BA does not include the ferrous metal scraps (ranging $5-8 \cdot 10^3$ t/a) that are recovered by a rough magnetic separation after quenching and re-melted for reuse; the ferrous metal fraction is not considered in this study. The FA samples are further divided in different categories depending on the technology of the air pollution control system (Funari et al., 2016b). Where possible, four categories of FA were collected: at the first step without any treatment (FAU), after the electrostatic precipitator (FAE) and after bag filters chemically assisted with soda (FAS) and lime (FAL) additives. Since sampling materials from incineration waste cannot display the variability inherent of a given plant over time, we assume that each sample is representative of the MSWI ash category of each MSWI plant for the year at sampling (2013). Therefore, spatiotemporal variations of MSWI ashes are not assessed in this work, but rather our samples serve as an averaged reference for the north Italian region. Moreover, these samples are assumed to be a reliable reference as we are referring to MSWI plants that, altogether, burn more than 25% total waste capacity of the region (ISPRA, 2018).

The sample-set is composed of 47 samples, including 8 magnetic extracts of selected BA and FA materials. The analysis of magnetic extracts allowed to characterise better a weakly magnetic fraction (hereafter “more diamagnetic fraction” for simplicity) and a more magnetic one (hereafter “magnetic extract”) of the same specimen.

2.2. Samples pre-treatment

The material pre-treatment included 1) drying at 40 °C for one week; 2) hand-sorting and removal of the largest metallic fragments, e.g., partly melted screws, bolts and cans, found in the BA samples; 3) homogenisation with an agate rotating mill disk. Magnetic and diamagnetic extracts were collected using a Frantz magnetic separator by imparting a 1.1 A current in the laminar isodynamic region and a +15° side slope of the chute (as in Funari et al., 2018) as to refer as magnetic separation.

2.3. Magnetic measurements

A range of magnetic measurements was conducted on triplicate samples at the Institute of Marine Sciences of the National Research Centre (CNR-ISMAR, Bologna). Magnetic susceptibility at room temperature was measured at two different frequencies (0.47 and 4.7 kHz) by using a dual frequency MS2B Bartington meter (Bartington Instruments Ltd, UK). The difference between the two measurements was used to calculate the frequency dependence of susceptibility (κ_{fd}%). The calibration of the instrument was checked using a permalloy standard as magnetic reference material. Samples of dried powder were laid down and gently compacted in cubic plastic boxes of 8 cm^3 volume. Mass specific magnetic susceptibility (χ) was calculated dividing the volume susceptibility (κ), previously corrected for the drift, by the sample mass. An induced anhysteretic remanent magnetization (ARM) was imparted by an AGICO LDA-3A AF demagnetizer to all samples using a peak alternating field (AF) of 100 mT with a biasing superimposed direct current (DC) field of 0.1 mT parallel to the AF; the mass-specific susceptibility of ARM (χ_{ARM}), expressed in m^3/kg, was calculated after mass-normalisation and bias DC field correction. Isothermal remanent magnetization (IRM) experiments were performed using an ASC IM-30 pulse magnetizer. An IRM up to 1.0 T was induced, followed by a reverse field of IRM in five steps up to 0.4 T. The IRM acquired in a field of 1.0 T was regarded as the saturation IRM (SIRM). From the measured value, expressed in A/m, the mass magnetization is calculated by dividing for volume and mass weight of the sample in Am^2/kg. The IRM experiments allowed the calculation of additional parameters such as the coercivity of remanence (B_{0cr}) and the S-ratio, defined as IRM_{-300mT}/SIRM (Maher, 1988), where IRM_{-300mT} is the backfield IRM at a field of 300 mT. Major hysteresis loops and backfield curves at room temperature were measured on selected samples, using a MicroMag Princeton Measurements Vibrating Sample Magnetometer (VSM) with a nominal sensitivity of $5 \cdot 10^{-9}$ Am^2 at the Institute for Rock Magnetism (IRM, University of Minnesota). The general interpretation of the room-temperature magnetic parameters (Moskowitz et al., 2015; Thompson and Oldfield, 1986) is given as supplementary information (S1; Table S1).

2.4. Geochemical and mineralogical analysis

The chemical and mineralogical composition was analysed at the Department BiGeA (University of Bologna) and the Department of Physics and Earth Sciences (University of Parma) as complementary information to magnetic techniques. Additional details on the chemical and mineralogical analysis can be found in S2 and S3, respectively. Particles morphology and dimensions were observed at different magnification on a Scanning Electron Microscope (SEM), JEOL JSM-6480LV high-performance, capable of working at variable pressure with secondary electron and backscattered electron imaging detectors. The bulk chemical composition was determined by X-ray fluorescence (XRF) on pressed powder pellet (φ37 mm) in a boric acid binder, using 3 g of the dried and milled sample. A wavelength-dispersive spectrometer (WD-XRF; PANAlytical, Axios 4000) was used for the analysis. The estimated precision for major and trace element determinations are better than 5% except for concentrations detected as low as 10 mg/kg (10–15%). After correction for the Loss on Ignition (LOI), the following were determined by XRF (S2; Table S2): major elements (Si, Ti, Al, Fe, Mn, Ca) and minor and trace element (Cu, Ni, Mo, Pb, Zn, Zr), including metals considered as "critical" (Mg, Cr, Co, Ga, Nb, V, and the light rare earth elements La, Ce, Nd).

2.5. Statistical data analysis

We used multivariate statistics including Pearson's correlation coefficient analysis (PC), principal component analysis (PCA), and cluster analysis (CA) to investigate the relations between the measured geochemical and magnetic data (S4). PC analysis was used to determine the correlation between the measured chemical concentrations and other physical or chemical parameters. PCA incorporated both magnetic and geochemical data standardized into one unified comparison and allowed to use optimized minimum factors to explain the original data set. These statistical analyses were performed using the entire dataset except for magnetic extracts to avoid any dependence between variables and observations. To further evaluate the similarities between variables and confirm the observation from the PCA, cluster observations and cluster variables are calculated using CA, Ward's linkage and Euclidean distances.

3. Results

3.1. Bulk chemical composition

Major oxides concentration by XRF is given in Table 1. Minor and trace elements are reported in S2. The bulk chemical composition of BA and FA agree with earlier data from the literature (Bogush et al., 2015; Eusden et al., 1999; Funari et al., 2015). The main oxides in BA samples are SiO_2 and CaO with concentration averaging 30 g/100 g and 25 g/100 g, respectively. The major constituents of FA samples are Ca > Si > Al > Mg > K > Fe > Ti > P. Volatile elements such as Mo, Zn, and Pb are elevated in FA. Lithophile elements like Si, Al, and Ca, which form very stable oxides with a high boiling point, are higher in BA than in FA. The concentration of iron (as total Fe_2O_3) detected by XRF, averages 8 g/100 g for BA and 1.5 g/100 g for FA.

3.2. Mineralogy and morphology

The SEM/EDS analysis on BA and FA provides information on morphology, grain-size, and chemical composition of mineral phases as a semi-quantitative estimate. In both types of samples, the amorphous material is abundant and acts as a background matrix that surrounds euhedral phases, polycrystalline or sintered agglomerations of particles, and loose particles, in agreement with previous studies on MSWI ashes (A. P. Bayuseno and Schmahl, 2010; Bogush et al., 2015). The morphological observations disclose a wide range of shapes, e.g., spheres, flakes, prisms, needles, and irregular agglomerations (S3). Some particles can be very small, with diameters well below the micron range, overcoming the instrument resolution. The EDS chemical analysis (Fig. 1) shows that both single crystals and glassy groundmass contain a significant amount of Fe, Ti, and other substituting/pollutant elements (Zn, Pb, etc.). The magnetic extracts (Fig. 1b; Fig. S4) have a significant proportion of small (<5 μm) magnetic spherules, which are loose particles or attached to the surface of larger grains. Fe-bearing particles are abundant and, according to the EDS analysis, Fe occurs as iron oxide or associated with carbonates and silicates. Single particles with larger grain size (>100 μm) are rare and typically contain Si, Ca, Fe, S, and Al. Sparse, rounded particles, which appear brighter detecting contrast between areas of different chemical compositions, show on EDS spectra enhanced levels of Fe, Pb, Cr, Ti, or Zn plus variable amounts of S, Cl, Si, and Ca.

3.3. Basic magnetic properties

Table 1 shows the fundamental magnetic properties of BA and

Table 1
Dataset of magneto-chemical measurements (triplicate averages) showing selected room-temperature magnetic properties of BA and FA samples (including magnetic separates) from different MSWI plants, relative standard deviation (RSD) of susceptibility (χ), and major elements concentrations by XRF.

	MSWI n°	Sample mass *g*	X *$10^{-8}m^3/kg$*	RSD *%*	Kfd *%*	XARM *$10^{-6}m^3/kg$*	SIRM *$10^{-6}Am^2/kg$*	SIRM/χ *$10^{-3}A/m$*	χARM/χ *dimensionless*	B0cr *mT*	S-0.3 T *dimensionless*	MDFARM *mT*	Si *mg/kg*	Ti *mg/kg*	Al *mg/kg*	Fe *mg/kg*	Mg *mg/kg*	Ca *mg/kg*
Bottom ashes																		
BA1.1	1	7.95	219.9	1.3	2.0	43.745	253,282	115.2	19.9	41	0.95	11	183,292	8661	58,174	69,925	16,080	127,378
BA1.2		7.00	195.3	1.2	2.5	40.849	224,143	114.8	20.9	42	0.97	10	171,330	6074	54,083	65,961	18,250	136,962
BA1.3		6.86	209.6	1.2	2.4	39.491	229,273	109.4	18.8	43	0.97	12	172,924	6658	54,029	66,703	18,495	142,536
BA1.4		8.81	208.6	0.3	2.3	44.588	217,198	104.1	21.4	39	0.96	12	174,518	7242	53,976	67,445	18,740	148,109
BA1.5		8.24	301.1	0.7	1.2	51.195	389,648	129.4	17.0	52	0.97	15	171,736	7599	54,439	69,728	16,129	125,578
BA1.6		6.06	242.9	0.3	2.9	45.592	279,183	115.0	18.8	42	0.96	12	166,476	7741	55,048	70,844	15,474	125,264
BA1.7		6.95	207.8	0.3	2.6	46.035	227,287	109.4	22.2	44	0.96	13	154,305	6548	52,894	69,813	16,430	135,056
BA2.1	2	8.12	232.2	1.4	1.4	29.996	217,053	93.48	12.9	42	0.98	13	129,144	6102	44,365	52,955	11,552	154,273
BA2.2		6.41	189.8	0.5	1.4	24.969	198,151	104.4	13.2	42	0.96	10	136,810	7145	49,273	48,325	12,209	185,623
BA2.3		6.27	133.6	0.8	1.7	22.885	155,948	116.8	17.1	44	0.97	14	131,699	6450	46,001	51,412	11,771	164,723
BA2.4		7.69	221.1	4.2	1.4	31.148	223,165	100.9	14.1	37	0.95	8	129,084	6494	42,876	50,642	11,762	157,316
BA2.5		7.03	120.2	0.7	1.7	18.272	129,054	107.3	15.2	41	0.97	11	147,118	6239	50,384	64,328	15,906	128,547
BA2.6		9.36	358.0	1.8	1.3	44.028	337,191	94.20	12.3	39	0.96	13	132,947	6820	46,075	49,483	11,985	171,469
BA2.7		8.02	225.1	0.6	1.3	30.729	219,118	97.34	13.7	36	0.96	14	133,007	6427	47,564	51,797	11,776	168,426
BA2.8		7.09	137.2	0.7	1.9	21.414	136,751	99.67	15.6	38	0.96	12	129,144	6102	44,365	52,955	11,552	154,273
BA3.1	3	9.10	206.7	8.8	1.7	27.233	210,676	101.9	13.2	39	0.96	10	117,614	6295	25,298	54,860	13,589	241,281
BA3.2		8.53	193.0	8.6	1.5	28.331	211,509	109.6	14.7	38	0.97	11	117,614	6295	25,298	54,860	13,589	241,281
BA3.3		9.14	188.9	6.0	1.5	29.236	208,131	110.2	15.5	37	0.96	12	117,614	6295	25,298	54,860	13,589	241,281
BA3.4		11.79	195.8	4.0	1.3	28.304	194,704	99.47	14.5	36	0.95	10	165,997	3657	22,916	57,634	12,845	177,816
BA3.5		9.11	225.7	4.3	1.4	33.975	264,935	117.4	15.1	39	0.96	11	106,582	7673	28,526	55,606	14,594	247,141
BA3.6		7.17	195.2	25.4	1.1	28.355	209,135	107.1	14.5	44	0.94	13	80,264	7554	24,451	51,339	13,328	298,885
BA4.1	4	8.56	212.0	6.6	0.9	34.807	177,697	83.84	16.4	34	0.98	10	137,699	5216	34,154	42,620	20,203	204,688
BA4.2		8.07	198.4	5.7	1.4	26.626	178,920	90.17	13.4	37	0.96	11	137,699	5216	34,154	42,620	20,203	204,688
BA4.3		7.72	122.3	5.3	2.2	19.642	113,892	93.11	16.1	32	0.98	11	137,699	5216	34,154	42,620	20,203	204,688
BA4.4		6.48	162.5	2.0	1.5	22.743	153,746	94.59	14.0	43	0.97	15	172,494	3237	26,991	45,044	19,539	173,599
BA4.5		8.55	209.8	0.3	1.4	26.575	173,306	82.62	12.7	37	0.96	11	141,782	5575	39,375	49,451	23,519	184,891
BA4.6		7.08	132.0	0.6	1.6	22.896	125,180	94.85	17.3	38	0.95	11	98,822	6834	36,094	33,364	17,549	255,575
average			**201.7**	**3.5**	**1.7**	**31.987**	**209,566**	**103.9**	**15.9**	**40**	**0.96**	**12**	**131,699**	**6658**	**58,174**	**69,925**	**16,080**	**127,378**
Magnetic separates																		
BA2.D *more diamagnetic*	2	1.34	32.38	1.6	6.4	8.011	59,820	184.7	24.7	47	0.96	15	91,623	6594	56,629	48,262	15,077	197,256
BA3.D *fraction*	3	2.24	38.15	0.6	5.5	9.765	63,462	166.3	25.6	48	0.96	15	123,411	7194	55,570	46,164	16,283	260,863
BA2.M *magnetic extract*	2	5.24	1696.2	0.3	2.6	147.585	1,012,054	59.7	8.70	32	0.96	24	66,380	4196	31,225	251,102	21,107	121,498
BA3.M	3	4.18	1204.7	0.4	1.4	130.996	865,166	71.8	10.9	32	0.97	22	64,978	4796	33,342	226,621	25,329	150,086
Fly ashes																		
FAU1.1	1	7.72	40.09	0.5	1.9	7.683	37,971	94.7	58.2	34	0.95	7	64,796	7839	27,522	16,091	32,481	177,980
FAU1.2		8.57	43.07	0.9	2.8	8.516	41,243	95.8	18.0	32	0.94	9	64,796	7839	27,522	16,091	32,481	177,980
FAS1.1		4.67	2.497	0.3	6.6	0.659	1700	68.1	83.6	45	0.94	12	6536	519	1820	1600	3393	13,755
FAS1.2		5.24	2.285	0.3	6.3	0.671	1348	59.0	16.6	41	0.94	12	6536	519	1820	1600	3393	13,755
FAU2.1	2	6.14	16.35	4.8	4.2	9.509	10,905	66.7	26.4	31	0.92	7	65,371	9150	31,528	11,717	11,608	193,085
FAU2.2		7.89	16.76	0.2	3.6	3.024	11,420	68.1	29.4	32	0.91	8	65,371	9150	31,528	11,717	11,608	193,085

FAL3.1		3	5.72	13.91	0.3	3.1	2.511	8948	64.3	19.2	34	0.93	9	23,645	3419	12,088	6769	5902	217,767
FAL3.2			5.37	13.55	1.4	3.0	3.342	7321	54.0	19.8	31	0.92	9	23,645	3419	12,088	6769	5902	217,767
FAU3.1			6.76	18.97	1.0	3.7	3.818	13,719	72.3	18.1	25	0.93	7	76,293	10,200	38,381	13,091	12,517	213,699
FAU3.2			6.97	20.08	1.0	3.7	5.041	16,356	81.5	24.7	31	0.93	8	76,293	10,200	38,381	13,091	12,517	213,699
FAE4.1		4	4.46	30.02	0.8	3.0	25.092	25,047	83.4	20.1	32	0.95	67	65,652	7009	27,751	13,818	8465	132,233
FAE4.1			6.06	24.66	2.0	1.6	4.095	20,133	81.7	25.1	34	0.95	9	65,652	7009	27,751	13,818	8465	132,233
	average			**20.19**	**1.1**	**3.6**	**6.163**	**16,343**	**81.0**	**29.9**	**33**	**0.93**	**14**	**131,699**	**6548**	**58,174**	**69,925**	**16,080**	**127,378**
Magnetic separates																			
FAU2.D	*more diamagnetic*	2	2.73	7.043	1.7	5.2	1.353	3238	46.0	19.2	26	0.87	0.1	44,877	4796	24,874	6994	4825	163,665
FAU3.D	*fraction*	3	2.32	3.730	3.9	4.0	0.876	1652	44.3	23.5	24	1.00	4	32,723	2398	41,281	699	2412	142,939
FAU2.M	*magnetic extract*	2	2.77	11.76	0.2	4.3	2.618	6893	58.6	22.3	26	0.91	16	37,397	10,791	2646	17,486	43,421	157,233
FAU3.M		3	0.98	21.95	1.0	2.8	6.258	15,280	69.6	28.5	25	0.92	15	65,445	7194	5292	18,885	41,611	129,360

FA samples collected from the four investigated MSWI plants. Each value results from triplicate analysis. The mass-specific magnetic susceptibility (χ) values range 1.20–3.58 · 10^{-6} m^3/kg for BA samples and 2.3–43.1 · 10^{-8} m^3/kg for FA samples. These data are consistent with previous magnetic measurements of MSW incineration residues and landfill leachates (Funari et al., 2016b; Funari et al., 2018; Huliselan et al., 2010), while partly lying below the χ measurements of other combustion residues such as coal fly ashes, coke dust, and residues after lignite burning (Lu et al., 2009; Magiera et al., 2011; Szuszkiewicz et al., 2015). The intensities of the measured susceptibility are roughly proportional to the average iron contents determined by XRF, indicating Fe-bearing minerals are chief carries of the magnetic signal. Although there is no clear correlation between BA samples and the corresponding FA produced from the same MSWI plant, chemically treated fly ashes (i.e., FAS and FAL) experienced lower χ values. According to the coefficient of variation for χ, the dispersion of χ measurements is much higher in BA than in FA, corroborating the hypothesis that samples' heterogeneity has a critical effect on BA materials during sampling (Funari et al., 2015).

A characteristic feature of MSWI ashes is the relatively high percentages of κ_{fd}, greater than 6% for a few samples, in agreement with previous works (Funari et al., 2016b; Funari et al., 2018). The BA samples show lower κ_{fd} values compared to the FA ones. Samples from the FAS group, only available for MSWI-1 plant, recorded the highest κ_{fd} percentages. The measured κ_{fd} values for FA samples markedly differ from other anthropogenic solid residues originated from industrial processes, such as, thermoelectric power plants and steelworks, which gave lower κ_{fd}% values (Jordanova et al., 2006; Magiera and Strzyszcz, 2000). Particular types of materials of both geogenic and anthropogenic origin like Chinese loess, pedogenetic soil horizons, urban topsoils, street dust, and urban particulate matter, have levels of κ_{fd}% comparable to MSWI samples (Maher and Taylor, 1988; Wang et al., 2010; Zhu et al., 2013). The κ_{fd} parameter can reflect the presence of very fine ($d < 0.03$ μm for magnetite) ferro(i)magnetic grains in the SP state. As the interpretation of κ_{fd}% fluctuations is hardly reliable for anthropogenic materials, the κ_{fd} parameter can give a qualitative indication of ultrafine-sized grains contained in MSWI ashes. Moreover, frequency-dependent susceptibility measurements with Bartington susceptibility meter are unstable, and triplicate analysis can provide no more than preliminary estimates. A reliable estimation of the SP fraction should rely on more robust means like temperature-dependent data (Funari et al., 2018; Hunt et al., 1995).

The SIRM/χ ratio is another grain-size sensitive magnetic parameter. For the anthropogenic ferro(i)magnetic grains contained in MSWI samples, this ratio ranges from 0.05 to 0.13 A/m (Table 1). Such a range is characteristic for coarse-grained MD stoichiometric magnetite with grains diameter greater than 5 μm (Thompson and Oldfield, 1986). The diagnostic significance of the SIRM/χ ratio, however, can be overwhelmed by mixed magnetic mineral assemblages, especially hybrid mineral compositions and naturally incompatible assemblages as acknowledged to occur in MSWI ashes (Eusden et al., 1999). SIRM and χ well linearly correlate ($R^2 = 0.96$) for all MSWI samples (Table 1, Fig. 1), indicating that the ferro(i)magnetic phases are the dominant magnetic minerals (Oldfield, 1991). The anhysteretic susceptibility (χ_{ARM}) ought to provide constraints on the grain-size of ferro(i) magnetic phases of SD and PSD grains (King et al., 1982; Maher, 1988), mostly regardless of MD-sized grains. The most important magnetic grain-size is relatively small according to the χ_{ARM} values: low for the entire dataset (up to 51 · 10^{-6} m^3/kg) and minimal for FA samples (down to 0.7 · 10^{-6} m^3/kg). These figures for χ_{ARM} are even lower than those reported by Maher (1988) for

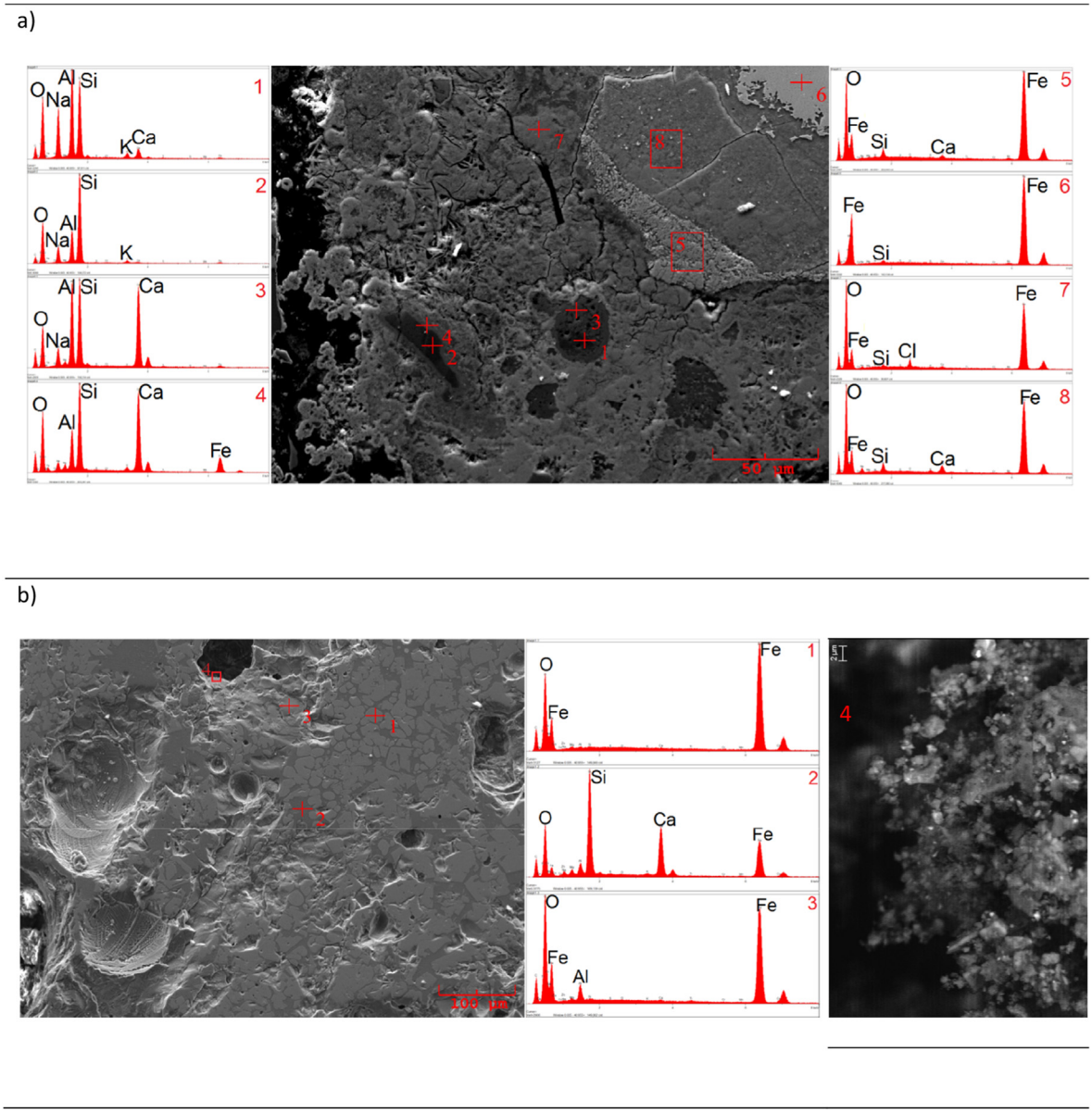

Fig. 1. SEM micrographs of FA (a) and BA (b) samples complemented with EDS spectra of the shooting point or zoomed area (point 4).

the finest grain-sizes of synthetic magnetites ("MT series", 0.012 μm < d < 0.017 μm). This does not necessarily mean that all or some particles occurring in MSWI ashes are below the SD threshold but indicates that the diagnostic characteristic of χ_{ARM} values is hampered, e.g., by the clumping of grains of different grain-sizes or mixed magnetic mineral assemblages. The χ_{ARM} vs χ plot in Fig. 1 shows a good correlation ($R^2 = 0.84$), indicating that the susceptibility enhancement is related to the presence of SD particles. The generally low χ_{ARM}/χ ratios (around 20) coupled with the measured κ_{fd}% can reflect the need to explore an eventual SP enrichment by other means.

The B_{0CR} of our samples of MSWI ashes ranges from 25 to 52 mT and averages 33 mT and 40 mT for FA and BA samples, respectively. The range of values of B_{0CR} reflects the absence of large grains in the MD state as well as a significant amount of high coercivity materials (e.g., hematite) (Thompson and Oldfield, 1986). High B_{0CR} and low $S_{-0.3T}$ values typically relate to increased hematite contents. Here, a relatively high B_{0CR} opposes with S-ratios close to 1, so the hypothesis of an important contribution of hematite to the remanence cannot be fully sustainable. It is reasonable that the coercivity enhancement given by hematite, most likely sums with the contribution of sulphur minerals or other high coercivity phases, not necessarily euhedral and in stoichiometric equilibrium, occurring in MSWI ashes (A. P. Bayuseno and Schmahl, 2010; Bogush et al., 2015) to give high $S_{-0.3T}$ values. As such, these values seem compatible with ferro(i)magnetic minerals, such as SD magnetite, acicular magnetite, oxidised magnetite, and iron sulphides. The median destructive field of ARM (MDF_{ARM}) usually increases with decreasing grain-sizes, but things become more complicated in SP- and coarse-MD-dominated assemblages (Maher, 1988). The effect of large MD grains on the B_{0CR} is likely overwhelmed by that of grains in a PSD (<1 μm) or SP (<30 nm) state so that the B_{0CR} parameter is unable to conform to MDF_{ARM} values and to detect grain-size.

The measured MDF_{ARM} values narrowly between 11.7 mT (FA average) and 13.7 mT (BA average) point to both coarse MD and

ultrafine SP grains because the ARM stability of some sub-micron magnetites increases with increasing grain-sizes in a certain MDF_{ARM} values range (~10–29 mT, (Maher, 1988)). The magnetic extracts of both BA and FA samples behave similarly to the corresponding original materials, showing comparable SIRM/χ and χ_{ARM}/χ ratios. Anomalies arise for the mineralogy-sensitive parameters like B_{0CR}, $S_{-0.3T}$, and MDF_{ARM}, which possibly indicate partitioning of the primary mineralogical assemblage. On the contrary, κ_{fd}, χ_{ARM} and SIRM values reported for MSWI samples are sensitive to magnetic grain-sizes.

Both FA and BA samples monotonically produce tall, thin hysteresis loops typical of a dominant contribution of low coercivity ferromagnets such as, magnetite, very little in dimensions (Thompson and Oldfield, 1986) or maybe MD/coarse magnetite adding to the smaller fractions, as previously observed for MSWI ashes (Funari et al., 2018). The samples from magnetic extraction differ in height, due to changes in the saturation of magnetization, but not in shape (S1; Fig. S1), indicating that specific quantity of magnetic minerals is stimulated by a 1.1 A current during magnetic separation.

4. Discussion

4.1. Correlation between variables and statistical data analysis

Pearson's correlation coefficients help to give a rapid picture of the inter-element relationship. Pearson's correlation coefficients show that Fe and Si concentrations significantly correlate to magnetic susceptibility, followed by Mn, Cu, Al, La, Ce, and a significant negative correlation is found for Zn and Pb. In particular (S4), silicon positively correlates with Fe (PC = 0.917) and Al (PC = 0.802), with a significant negative correlation with Zn (PC = −0.830). The correlations Ni–Ga and Ce–Co are apparent (PC > 0.85) possibly due to the legacy of some technogenic materials feeding the MSWI combustors. Using the BA population of samples for the same correlation analysis (Table S4), silicon negatively correlates with Ca (PC = −0.830), iron with Mo, Ni, Nb (PC > 0.7). For FA population, on the other hand, the PC shows a close association between Si, Ti, Al, and Fe as well as positive correlations between chalcophile elements (Ga, Pb, Zn, Cu, Ni). Moreover, Zn and Ni have a significant negative correlation with Si, Al, Ti, and Fe as a likely consequence of their different geochemical behaviour in the combustion chamber.

PCA was performed to further discern relationships and grouping among the analytical observations, namely using both magnetic and geochemical data (Table 2, and S4). The PCA reported in Table 2, designates four components (PC1-4) explaining 77.2% of the cumulative variance in the MSWI ashes sample-set (BA and FA altogether). PC1 accounted for 42.8% of the variance, indicating it as the chief controlling factor of the metal distribution into the samples.

According to the scores of first principal component and the Pearson's Correlation between elements (Table S4), the positive loading of PC1 corresponds to the elements Si, Al, Fe, Mn, Cu, Ce, Nd and the magnetic parameters, χ and S-ratio, as shown by the loading plot (Fig. S8). The second principal component explains about 21% of the variance; the scores are elevated for Zn, K, Pb, Mo, and κ_{fd}% and are negative for Ca (PC2 in Table 2). The third component relates the negative Al and Mg and shows high scores, e.g., Cr, La, Nb. In the fourth principal component, Mn, Zr, Cr, Ti, Al, and a single magnetic parameter, B_{0cr}, have a significantly high score. The statistical analysis suggests that some of the metals are related to magnetic properties. A similar association has been interpreted as the effect of the magnetic particle size for heavy metal contaminated soils (Song et al., 2011).

4.2. Understanding the magnetic grain size of MSWI sample-set

Magnetic ratios and diagrams can provide additional information on grain-size and mineralogy of the MSWI samples, bypassing the assumptions and limitations of the basic magnetic parameters. So combining magnetic parameters and taking insights from measurements on magnetic/diamagnetic extracts are desirable to disentangle mixed magnetic mineral assemblages and the ambiguities concerning grain-sizes.

The plot of SIRM and χ in Fig. 2 shows most of the data along the diagonal of the diagram, indicating that the concentration dominated the magnetic properties, with only minor role from the grain-size. The BA samples are more scattered than FA samples, indicating a more complicated mineral assemblage and greater heterogeneity of grain-sizes respect with FA materials. Furthermore, the content of ferro(i)magnetic minerals increases diagonally to the top-right corner. Samples shifted to the right of the diagonal, characterized by low SIRM and moderate susceptibility, are partly influenced by paramagnetic minerals. Data placed in the upper part of the diagram (SIRM > 200×10^{-3} Am^2/kg) in the right indicate samples with substantial contributions of coarse MD-magnetite, SP-magnetite, or a combination of both (Funari et al., 2018). These trends suggest that in particular BA samples are affected by an association of different grain-sizes.

Fig. 3 shows the standard bilogarithmic SIRM vs κ_{lf} plot that is used to further constrain the observation concerning magnetic grain-sizes. The grain-size thresholds refer to fundamental magnetic studies on natural and synthetic magnetites (Thompson and Oldfield, 1986). BA, FA, and the corresponding samples of magnetic extracts are reported. Similarly to Fig. 2, the plot of Fig. 3 indicates high concentrations of ferro(i)magnetic minerals diagonally increasing towards the top-right. The BA samples clearly cluster above FA samples, indicating a higher concentration of magnetite, as previously indicated in Fig. 2. Conversely, the FA samples from bag filters, i.e., FAS and FAL, have lower magnetite concentrations (<0.01 wt %). The plot of total iron by XRF, as Fe_2O_3, vs χ (Fig. 3, inset) shows similar clusters of data and suggests that the concentration of iron is directly related to the presence of ferro(i) magnetic minerals. According to the reference lines, the majority of MSWI samples data lie within the grain-size interval 1–8 μm, while the FA samples from bag filters and several samples subjected to magnetic separation seem slightly coarser than 8 μm. However, variable hematite to magnetite ratios and increasing concentrations of paramagnetic minerals can cause anomalies along abscissa and ordinate, respectively, as a direct consequence of the observed bias on the magnetic parameters more sensitive to mineralogy (Table 1). The slightly coarser grain-sizes of FA samples compared to the most of BA samples might be an artifact tied to the higher hematite to magnetite ratio (relatively high B_{0cr} and $S_{-0.3T}$), or to measurement errors, which are increasing due to the lower magnetic concentration in the FA samples. In a SIRM vs κ_{lf} plot, moreover, the fact of having MD magnetites and/or high concentrations of the SP fraction may shift the data: SP have high susceptibility and low or zero SIRM, MD have decreasing SIRM values for coarser grains. Although the χ_{ARM} vs SIRM measures are unreliable for SP/PSD-dominated assemblages and suffer the highest magnetization levels, the χ_{ARM} vs SIRM plot may be considered for comparison (S4; Fig. S12). It seemingly helps to discriminate BA from FA samples. The increase in χ_{ARM}/SIRM ratio in the higher magnetization levels suggests that these changes are associated with changes in the grain-size of the magnetic phases (Maher, 1988; Vigliotti et al., 1999; Yang et al., 2007), especially for several BA samples (i.e., those deriving from MSWI plant 1 and 4; Table 1). However, the contribution of the diamagnetic (i.e., mainly Ca-carbonates) fraction can lead to misinterpreting the recorded values of susceptibility

Table 2
–Principal component factor scores and eigenvalues of the correlation matrix. Bold highlights the notably positive scores for each component.

Variable	PC1	PC2	PC3	PC4
Eigenvalue	13.259	6.545	2.307	1.831
Proportion of variance	0.428	0.211	0.074	0.059
content				
χ	**0.239**	−0.088	0.058	0.123
κdf	−0.18	**0.243**	−0.076	0.001
κ_{ARM}	**0.252**	−0.038	0.002	0.025
SIRM	**0.245**	−0.062	0.07	0.096
SIRM/χ	**0.24**	−0.05	0.065	−0.061
B_{0cr}	0.177	0.144	0.057	**0.245**
S-ratio	**0.215**	−0.032	0.039	0.18
MDF	0.014	0.04	0.199	−0.151
Si	**0.241**	−0.095	−0.134	−0.012
Ti	0.036	−0.184	−0.173	−0.513
Al	**0.208**	−0.039	−0.277	−0.321
Fe	**0.262**	−0.057	0.009	0.042
Mg	0.084	−0.117	−0.311	−0.002
Ca	−0.01	−0.331	0.04	0.04
Mn	**0.206**	0.016	−0.086	**0.254**
K	−0.181	**0.273**	−0.004	0.064
P	0.181	**0.226**	−0.143	−0.101
Cu	**0.221**	0.122	−0.158	−0.053
Cr	0.1	0.154	**0.254**	−0.29
Ce	**0.206**	0.193	0.028	−0.206
Co	0.192	0.197	0.012	−0.068
Ga	0.14	**0.294**	−0.155	0.079
La	0.154	0.016	**0.413**	−0.016
Mo	−0.103	**0.3**	−0.031	−0.094
Nb	0.088	**0.238**	**0.341**	0.163
Nd	**0.217**	0.072	**0.292**	−0.164
Ni	0.129	**0.323**	−0.071	−0.006
Pb	−0.136	**0.255**	−0.227	−0.025
V	0.167	0.148	−0.263	−0.068
Zn	−0.202	**0.244**	0.007	0.068
Zr	0.119	−0.038	−0.269	**0.442**

(Hrouda et al., 2013). Therefore, a correct estimation of grain-size is unlikely due to the complicated mineralogy and petrogenesis of MSWI ashes (Eusden et al., 1999). On a κ_{ARM} vs κ_{lf} plot (King et al., 1982) (Fig. 4), which is less affected by the sample mineralogy and more grain-size sensitive compared to the SIRM vs κ_{lf} plot, data may also become smeared out if clumping of different grain-sizes occurs. The King's plot indicates a prevalent grain-size around the 1 μm threshold. Magnetic extracts of BA samples are clearly placed on the top-right side of the plot in Fig. 4. The more diamagnetic BA fractions (i.e., BA2.D, BA3.D), FA magnetic extracts (i.e., FAU2.D, FAU3.D, FA2.M, FAU3.M), and a FAE sample plot beyond the 0.1 μm grain-size boundary (see also zoomed inset of Fig. 4). This suggests that the finest magnetic particles are possibly efficiently extracted from BA samples, while the effect of FA magnetic separation to the King's plot is the mere lowering of κ_{ARM} and shows limited potential for grain-size screening/separation.

It stands to reason that observational errors can be considered with good coverage of replicate measurements to enable magnetic models' ability to predict grain-size of anthropogenic materials: there is the need to be cautious when drawing conclusions from these trends confronted to the limited number of room-temperature magnetic observations available from the literature on thermally treated, urban waste.

Understanding magnetic mineral resources of the MSWI sample-set.

According to the bilogarithmic plot of Fig. 5 (Peters and Thompson, 1998), the MSWI samples lie at the boundary between pyrrhotite and magnetite/titanomagnetite. The plot also indicates a magnetic mineral assemblage composed by SD structures and rules out the presence of hematite, goethite, and greigite. The BA samples plot further to the upper right respect with the FA samples, signifying the probable presence of harder magnetic phases in BA materials. There is the likelihood that data points are biased towards the pyrrhotite area due to high concentrations of sulphur (assessed by SEM/EDS, S3) and mixing of hard/soft magnetic minerals.

The simultaneous presence of impure iron oxides, magnetic sulphide minerals (e.g., greigite, pyrrhotite), and other magnetic phases like certain magnetic hydroxides, carbonates, and silicates is highly probable. Elemental maps of concentration taken on polished sections by SEM/EDS confirm the hypothesis deriving from magnetic parameters. The elemental map for the magnetic extracts reveals a close association between iron, oxygen and potential substitutes in the crystal lattice of magnetic oxides (i.e., Mg), as well as between iron and sulphur. Oxygen lacks where sulphur markedly appears, indicating the presence of sulphides and, in addition, iron-rich carbonates and silicates are likely to occur due to the significant association of iron with Ca and Si, especially in FA magnetic extracts (Fig. 6).

Other graphical techniques for magnetic mineral identification

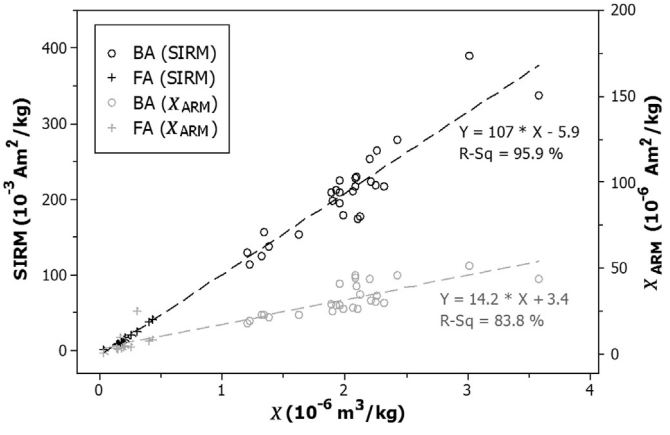

Fig. 2. Scatter plot of χ versus SIRM and χ_{ARM}. Samples are grouped by type (i.e., BA and FA), and the regression fits are shown for both variables along with equation and R-squared value.

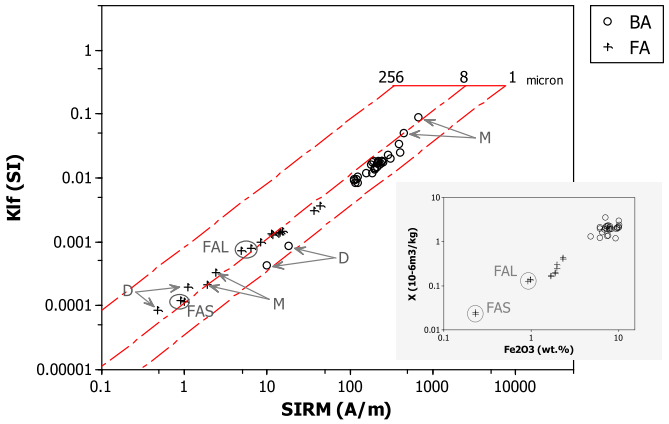

Fig. 3. The SIRM vs κ_{lf} plot of MSWI ashes. BA and FA samples scatter within the standard plot by Thompson and Oldfield (1986), which is based on 1000 natural samples and 25 magnetic extracts of natural samples. Please note that SIRM is expressed as A/m (without mass correction) to adhere to the standard plot. The red dashed lines are the grain-size threshold (values in μm). FA samples from bag filters (FAS and FAL) are circled. Samples after magnetic separation are also reported (M = magnetic extract; D = more diamagnetic fraction). The inset shows the iron concentrations (by XRF, conventionally given as Fe_2O_3) vs mass susceptibility (χ). (For interpretation of the references to colour in this figure legend, the reader is referred to the Web version of this article.)

proposed in the literature (Magiera and Strzyszcz, 2000; Peters and Thompson, 1998) have been tested (Fig. S13), but they suffered the peculiar measured values of MSWI ashes and appeared unsuitable. Nonetheless, recent studies on MSWI ashes reported the finding of mineralogical phases (Bayuseno and Schmahl, 2010; Bayuseno and Schmahl, 2011; Bogush et al., 2015) whose magnetic properties are known with confidence on numerous synthetic and natural samples (Moskowitz et al., 2015). Complementing the fundamental magnetic plots with chemical information using interpolated contours allows going deeper with mineralogical identification of MSWI samples and, as a consequence, to shed light on magnetic phases responsible for magnetic data variability. On the *SIRM/χ* vs B_{0CR} plot and the *SIRM/χ* vs MDF_{ARM} plot (Fig. 7), the fact that magnetic and diamagnetic extracts fall on opposite sides shows that such magnetic parameters act as mineralogical indicators for BA and FA, respectively. Therefore, they can help to assess the magnetic minerals which are extracted from both BA and FA samples after the magnetic separation. The *SIRM/χ* vs B_{0CR} plot of BA samples likely indicates the occurrence of magnetite and Mg-rich impure magnetite (e.g., magnesioferrite) (Fig. S5 in S3), while minerals like those from titanohematite/ulvospinel series and chalcophile elements partition in relatively more diamagnetic materials (Fig. 7). For FA samples, on the other hand, the top-right corner of the plot (Fig. 7; Fig. S6 in S3) indicates that the magnetic fraction likely experienced potential Ti > Mg(>Cr > Al) substitution of Fe in magnetites or other magnetic minerals (magnetic sulphides, magnetic carbonates). Overall, the effect of amorphous magnetic silicates or other magnetic alloys can be responsible for unaccounted magnetization on both BA and FA, so more data are needed to constrain the model better. Also, the glassy matrix of these residues might contain iron that is often underestimated but likely contribute to the magnetic response (S3; Fig. S7).

For the plots of Fig. 7, three magnetic variables (B_{0CR}; *χ; SIRM*) and data from magnetic/diamagnetic extracts are necessary to further constrain the chemical contouring in order to understand the magnetic minerals partitioning in the separates. A variety of different factors and processes can influence the analytical result of each variable (magnetic, chemical) at each sample site (MSWI plant feedstock, MSWI plant design), so statistical data analysis (S4) can help to identify which variable(s) is better representative of the samples. Data from magnetic separation are now excluded to avoid the effect from dependent variables (samples after magnetic separation likely affect the correlation with magnetic parameters, especially when interpolating chemical data; see S6). According to the PCA (Table 2), the first factor explains 44% of the total variance on a large number of variables. The measured magnetic parameters χ, SIRM, S-ratio, B_{0CR}, fall in the first component. On a CA performed using the PCA's first components (S4) five clusters are identifiable, and the latter (cluster V) discriminates BA from FA samples. This, in turn, suggests that a more homogeneous subset of variables can better explain the data structure, so, we consider BA and FA samples as two independent subsets of samples to successfully use the data integration method as a tool for metal prospecting in MSWI urban ores. The plot in Fig. 8, contoured as in Fig. 7, considers as a chemical indicator two magnetic variables from the PCA first component, B_{0CR} and $S_{-0.3T}$. The effect given from the higher magnetization is partly removed by using these magnetic parameters. As such, the interpolated maps of concentration overlying the plots are less prone to account for magnetic mineralogy while more sensitive to metal contents. To high $S_{-0.3T}$ values corresponds an enrichment of the critical element Mg for BA and FA samples, which is directly related to the probable occurrence of Mg-magnetites. In

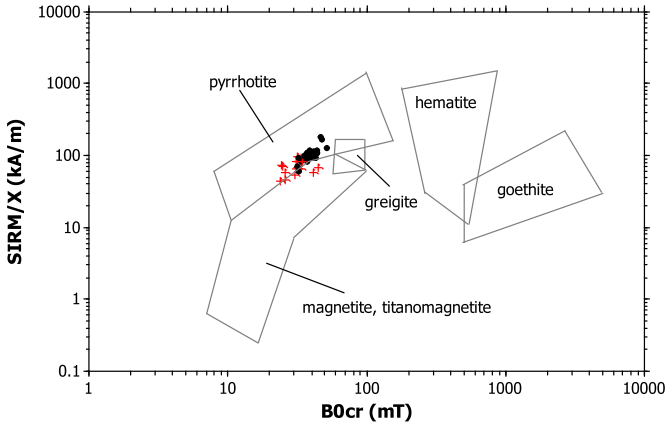

Fig. 5. SIRM/χvs B_{0CR} plot for qualitative identification of magnetic minerals (Peters and Thompson, 1998) showing BA and FA samples represented by circles and crosses, respectively.

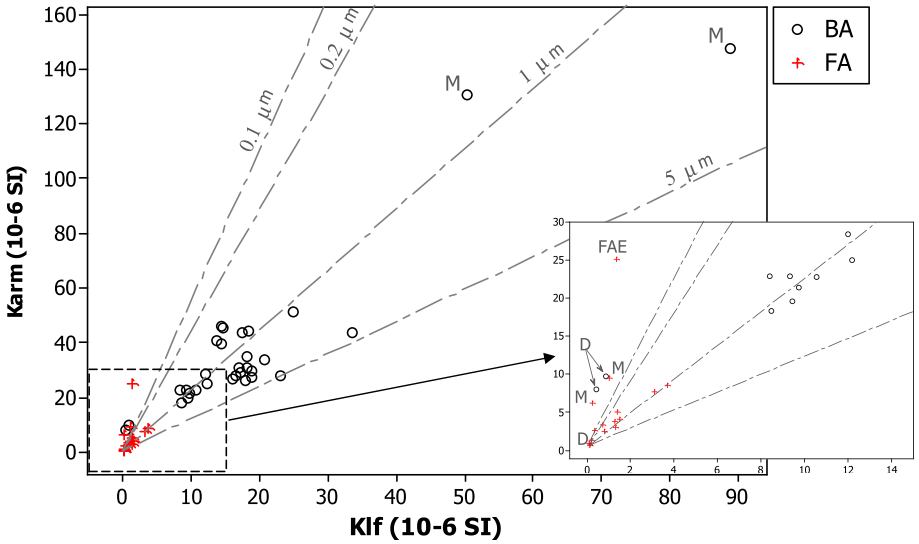

Fig. 4. Anhysteretic remanent magnetization of volume-specific susceptibility (κ_{ARM}) vs low-field susceptibility (κ_{lf}) for BA and FA samples. The grain size boundaries are estimated after King et al., (1982). The inset shows a zoomed area of the bottom-left side of the graph. For nomenclature, see Fig. 2.

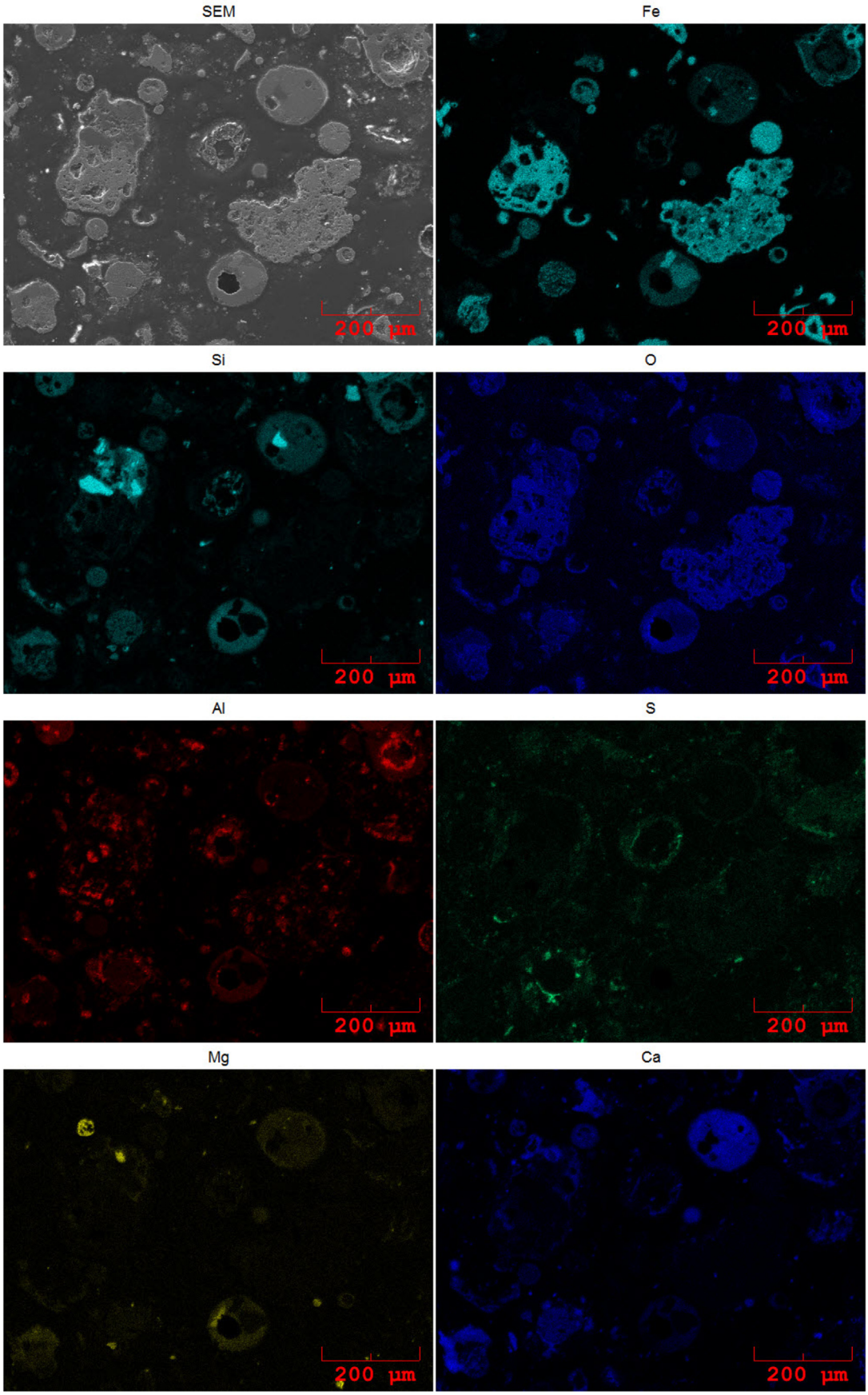

Fig. 6. Elemental map of FA magnetic extract ("FAU2.M").

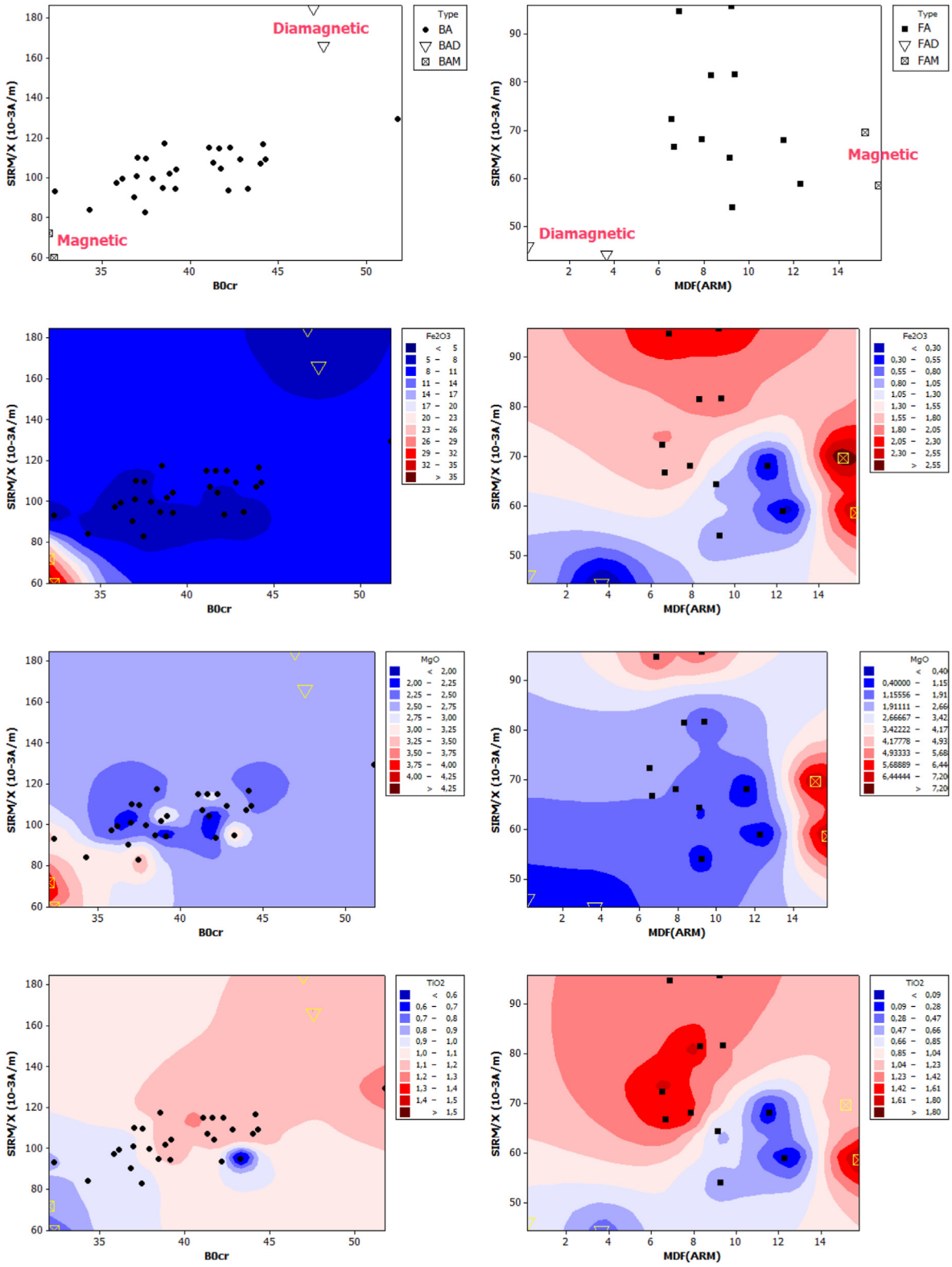

Fig. 7. Plot of SIRM/χ vs B_{0CR} (for BA samples, left column) and vs MDF_{ARM} (for FA samples, right column) coupled with IWD contouring of chemical concentrations. The plots show magnetic (squares), and diamagnetic (triangles) extracts as a reference.

FA sample-set high concentrations of critical elements, Nb and Ga, and toxic elements, Ni, relate to large $S_{-0.3T}$ and relatively low B_{0CR}. The rare earths, La, Ce, and Nd, seem to depend on the B_{0CR} value with divergent behaviour between BA and FA subsets; Ca, Nb, and Cr likely enrich based on $S_{-0.3T}$ and B_{0CR} ratios. Magnetic parameters demonstrated high potential for environmental magnetic studies (e.g., Zhang et al., 2011) however their application to waste management for resource prospecting was surmised quite recently for

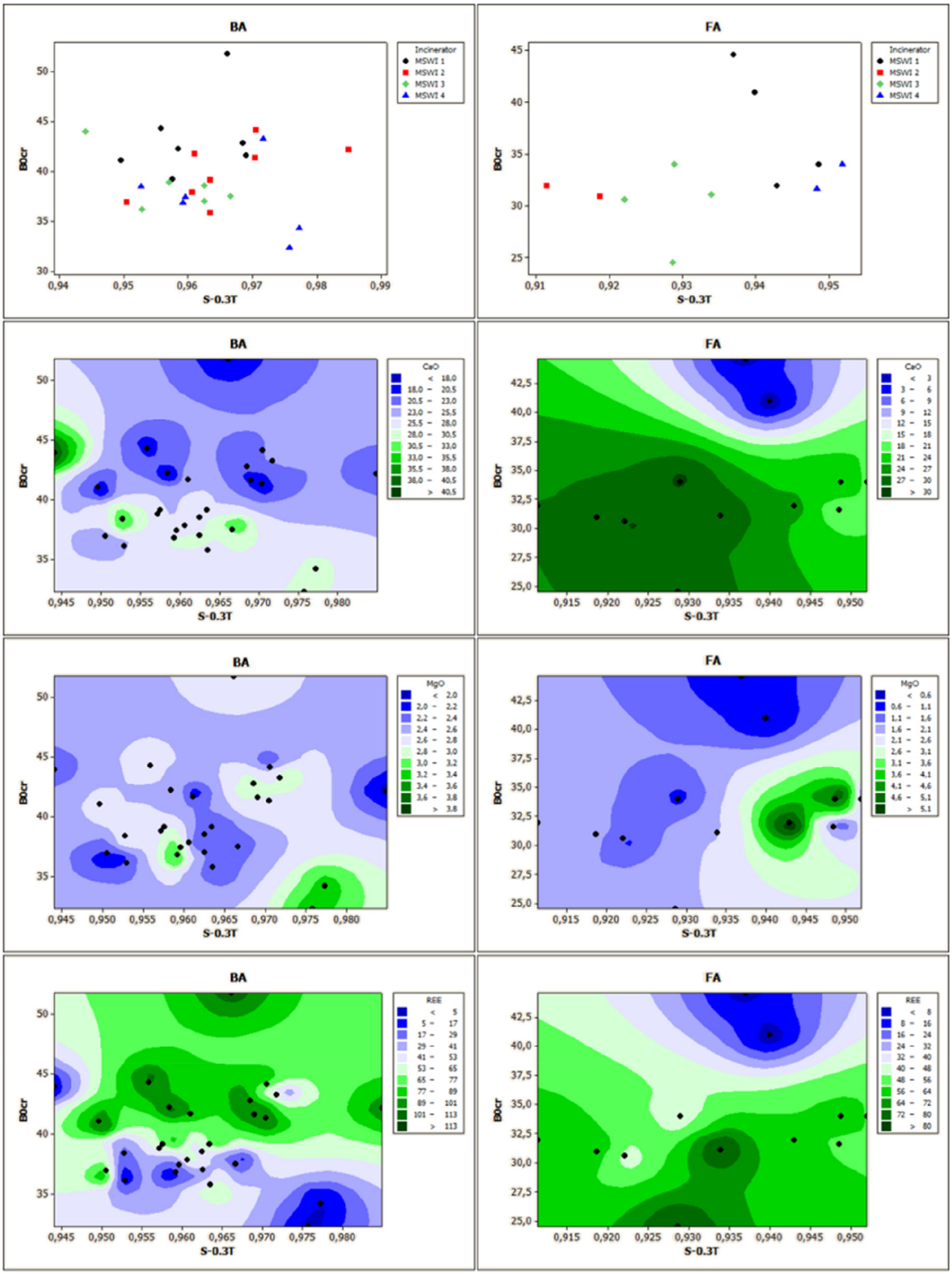

Fig. 8. $S_{0.3T}$ vs B_{OCR} plot of BA and FA samples coupled with IWD contouring of chemical concentrations. The two plots of the first row show the raw data points coloured according the different MSWI systems.

MSWI ashes (Funari et al., 2016b), and new data are wanted to understand the suitability for enhanced urban mining fully.

5. Conclusions and outlook

In this study, the correlation between geochemical data and

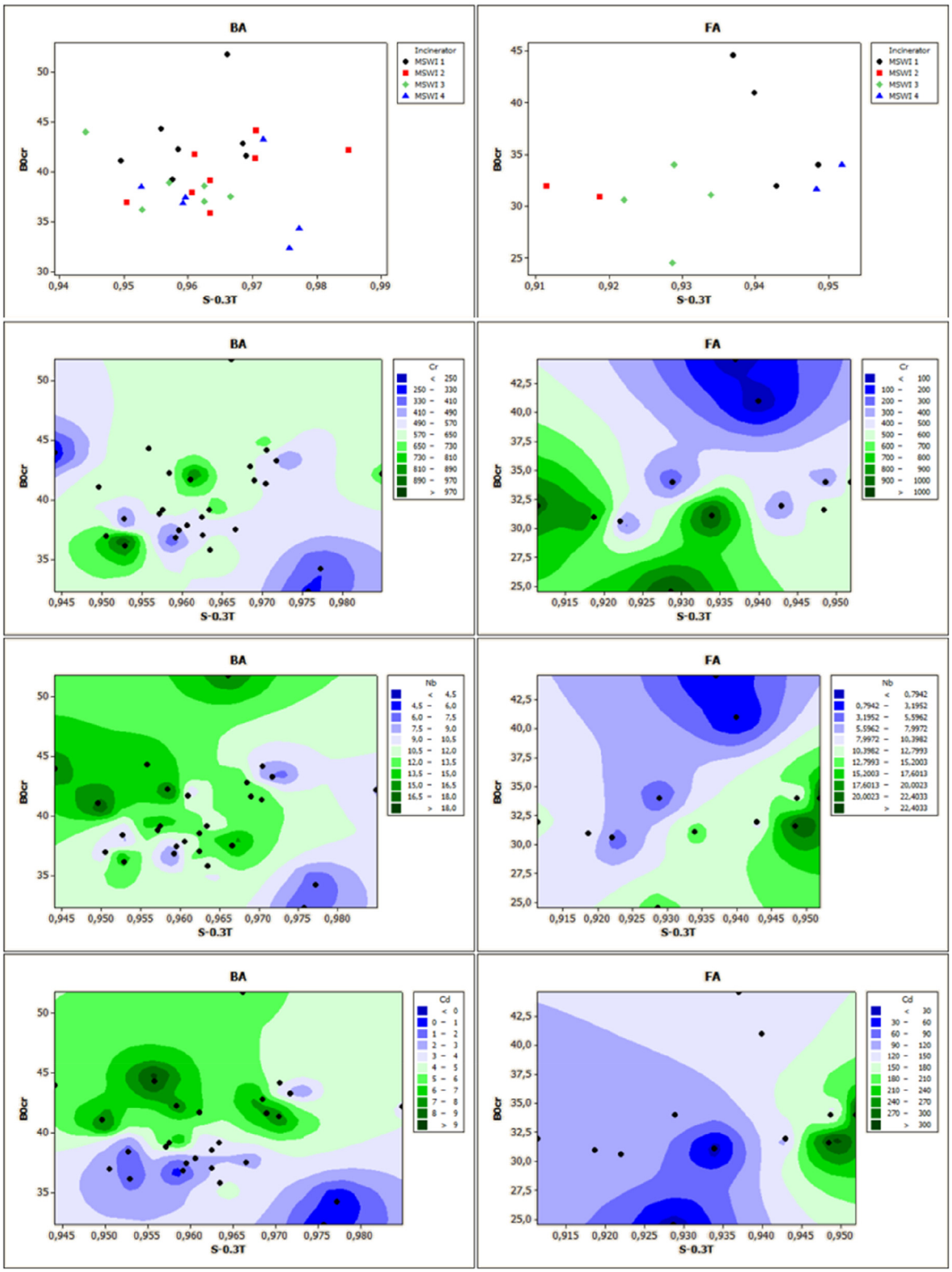

Fig. 8. (*continued*).

magnetic properties of Municipal Solid Waste Incineration (MSWI) ashes is seen as a strategic tool to help with resources supply and environmental assessment from bottom (BA) and fly (FA) ashes. A range of room-temperature magnetic measurements, chemical determination by XRF, and electron microscopy observations were performed on a collection of BA and FA from different MSWI facilities. Reporting magnetic methods integration to a geochemical study of anthropogenic materials was crucial to demonstrate that such models might help to predict impacts and resources related to MSWI ashes. The statistical data analysis showed evidence of the

nonlinear relationships amongst the input variables and helped to define the most significant magnetic parameters for the appraisal (i.e., χ, B_{0cr}, and the S-ratio). Magnetic methods are relocatable in the field and extremely sensitive, demonstrating a potential for urban mining. However, it would be worth producing new data from other case-studies to legitimise the magnetic method as a tool for prospecting valuable metals in the field of recycling anthropogenic materials. Besides appearing as niche methods to some extents, the magnetic methods used in this study can make possible a quick and cheap evaluation of the resource present in the MSWI bottom ash stockpile or other types of anthropogenic deposit. However, the magnetic susceptibility values measured in the lab must be preferred for further consideration especially when the only fine fraction is being focused. Overall, the results give confidence in integrated models' ability to predict metal enrichment and mineral segregation and, thus, informing the strategic analyses of valorisation of MSWI ashes. However, it is important to be cautious due to poor measurement coverage. There is a strong need for more observations at different MSWI sites in other countries to enable more reliable models with well-ascertained potential and limitations.

Acknowledgements

The authors gratefully acknowledge the assistance of Franco Corticelli, Lucilla Capotondi, Roberto Braga, Giorgio Gasparotto and Marzia Rovere during microscopy analyses. Part of this work was performed at the Institute for Rock Magnetism (IRM), University of Minnesota, thanks to an IRM Visiting Fellowship to V.F.; the IRM is a US National Multi-user Facility supported through the Instrumentation and Facilities Program of the National Science Foundation, Earth Sciences Division, and by funding from the University of Minnesota. Special thanks are due to Mike Jackson, Dario Bilardello, and the IRM research staff. The handling editor and three anonymous reviewers are thanked.

References

Bayuseno, A.P., Schmahl, W.W., 2010. Understanding the chemical and mineralogical properties of the inorganic portion of MSWI bottom ash. Waste Manag. 30 (8–9), 1509–1520. https://doi.org/10.1016/j.wasman.2010.03.010.

Bayuseno, A.P., Schmahl, W.W., 2011. Characterization of MSWI fly ash through mineralogy and water extraction. Resour. Conserv. Recycl. 55 (5), 524–534. https://doi.org/10.1016/j.resconrec.2011.01.002.

Bogush, A., Stegemann, J.A., Wood, I., Roy, A., 2015. Element composition and mineralogical characterisation of air pollution control residue from UK energy-from-waste facilities. Waste Manag. 36, 119–129. https://doi.org/10.1016/j.wasman.2014.11.017.

Brännvall, E., Kumpiene, J., 2016. Fly ash in landfill top covers – a review. Environ. Sci.: Process. Impacts 18, 11–21. https://doi.org/10.1039/c5em00419e.

Chaparro, M., Bidegain, J., Sinito, A., Jurado, S., Gogorza, C., 2004. Relevant magnetic parameters and heavy metals from relatively polluted stream sediments-Vertical and longitudinal distribution along a cross-city stream in Buenos Aires Province, Argentina. Studia Geophys. Geod. 48 (3), 615–636.

Commission, E., 2014. Report on Critical Raw Materials for EU*Rep*.

Englert, N., 2004. Fine particles and human health - a review of epidemiological studies. Toxicol. Lett. 149, 235–242.

Eusden, J.D., Eighmy, T.T., Hockert, K., Holland, E., Marsella, K., 1999. Petrogenesis of municipal solid waste combustion bottom ash. Appl. Geochem. 14 (8), 1073–1091. https://doi.org/10.1016/S0883-2927(99)00005-0.

Fellner, J., Lederer, J., Purgar, A., Winterstetter, A., Rechberger, H., Winter, F., Laner, D., 2015. Evaluation of resource recovery from waste incineration residues–the case of zinc. Waste Manag. 37, 95–103. https://doi.org/10.1016/j.wasman.2014.10.010.

Funari, V., Braga, R., Bokhari, S.N., Dinelli, E., Meisel, T., 2015. Solid residues from Italian municipal solid waste incinerators: a source for "critical" raw materials. Waste Manag. 45, 206–216. https://doi.org/10.1016/j.wasman.2014.11.005.

Funari, V., Meisel, T., Braga, R., 2016a. The potential impact of municipal solid waste incinerators ashes on the anthropogenic osmium budget. Sci. Total Environ. 541, 1549–1555. https://doi.org/10.1016/j.scitotenv.2015.10.014.

Funari, V., Bokhari, S.N., Vigliotti, L., Meisel, T., Braga, R., 2016b. The rare earth elements in municipal solid waste incinerators ash and promising tools for their prospecting. J. Hazard Mater. 301, 471–479. https://doi.org/10.1016/j.jhazmat.2015.09.015.

Funari, V., Mantovani, L., Vigliotti, L., Tribaudino, M., Dinelli, E., Braga, R., 2018. Superparamagnetic iron oxides nanoparticles from municipal solid waste incinerators. Sci. Total Environ. 621, 687–696. https://doi.org/10.1016/j.scitotenv.2017.11.289.

Hoesly, R.M., et al., 2018. Historical (1750–2014) anthropogenic emissions of reactive gases and aerosols from the Community Emissions Data System (CEDS). Geosci. Model Dev. (GMD) 11 (1), 369–408. https://doi.org/10.5194/gmd-11-369-2018.

Hrouda, F., Pokorný, J., Ježek, J., Chadima, M., 2013. Out-of-phase magnetic susceptibility of rocks and soils: a rapid tool for magnetic granulometry. Geophys. J. Int. 194 (1), 170–181. https://doi.org/10.1093/gji/ggt097.

Huliselan, E.K., Bijaksana, S., Srigutomo, W., Kardena, E., 2010. Scanning electron microscopy and magnetic characterization of iron oxides in solid waste landfill leachate. J. Hazard Mater. 179 (1–3), 701–708. https://doi.org/10.1016/j.jhazmat.2010.03.058.

Hunt, C.P., Banerjee, S.K., Han, J., Solheid, P.A., Oches, E., Sun, W., Liu, T., 1995. Rock-magnetic proxies of climate change in the loess-palaeosol sequences of the western Loess Plateau of China. Geophys. J. Int. 123, 232–244.

ISPRA, 2018. Rapport rifiuti urbani 2018. Istituto Superiore per la Protezione e la Ricerca Ambientale (ISPRA), ISBN 978-88-448-0928-7. ISPRA Rapporti 297/2018. http://www.isprambiente.gov.it/it/pubblicazioni/rapporti/rapporto-rifiuti-urbani-edizione-2018.

Jakšík, O., Kodešová, R., Kapička, A., Klement, A., Fér, M., Nikodem, A., 2016. Using magnetic susceptibility mapping for assessing soil degradation due to water erosion. Soil Water Res. 11 (No. 2), 105–113. https://doi.org/10.17221/233/2015-swr.

Jordanova, D., Jordanova, N., Hoffmann, V., 2006. Magnetic mineralogy and grain-size dependence of hysteresis parameters of single spherules from industrial waste products. Phys. Earth Planet. In. 154 (3–4), 255–265. https://doi.org/10.1016/j.pepi.2005.06.015.

King, J., Banerjee, S.K., Marvin, J., Ozdemir, O., 1982. A comparison of different magnetic methods for determining the relative grain size of magnetite in natural materials: some results from lake sediments. Earth Planet Sci. Lett. 59, 404–419. https://doi.org/10.1016/0012-821X(82)90142-X.

Li, H., Wang, J., Wang, Q., Tian, C., Qian, X., Leng, X., 2017. Magnetic properties as a proxy for predicting fine-particle-bound heavy metals in a support vector machine approach. Environ. Sci. Technol. 51 (12), 6927–6935. https://doi.org/10.1021/acs.est.7b00729.

Lu, S.G., Chen, Y.Y., Shan, H.D., Bai, S.Q., 2009. Mineralogy and heavy metal leachability of magnetic fractions separated from some Chinese coal fly ashes. J. Hazard Mater. 169 (1–3), 246–255. https://doi.org/10.1016/j.jhazmat.2009.03.078.

Maas, R., Grennfelt, P.E., 2016. In: Towards Cleaner Air. Scientific Assessment Report 2016, EMEP Steering Body and Working Group on Effects of the Convention on Long-Emission (Oslo).

Magiera, T., Strzyszcz, Z., 2000. Ferrimagneticminerals of anthropogenic origin in Soils of some polish national parks. Water, Air, Soil Pollut. 124, 37–48.

Magiera, T., Jabłońska, M., Strzyszcz, Z., Rachwal, M., 2011. Morphological and mineralogical forms of technogenic magnetic particles in industrial dusts. Atmos. Environ. 45 (25), 4281–4290. https://doi.org/10.1016/j.atmosenv.2011.04.076.

Maher, B.A., 1988. Magnetic properties of some synthetic sub-micron magnetites. Geophys. J. 94, 83–96.

Maher, B.A., Taylor, R.M., 1988. Formation of ultrafine-grained magnetite in soils. Lett. Nat. 336, 368–370. https://doi.org/10.1038/336368a0.

Moskowitz, B.M., Jackson, M., Chandler, V., 2015. Geophysical Properties of the Near-Surface Earth: Magnetic Properties, pp. 139–174. https://doi.org/10.1016/b978-0-444-53802-4.00191-3.

Oldfield, F., 1991. Environmental magnetism—a personal perspective. Quat. Sci. Rev. 10 (1), 73–85.

Peters, C., Thompson, R., 1998. Magnetic identification of selected natural iron oxides and sulphides. J. Magn. Magn Mater. 183, 365–374.

Quina, M.J., Bontempi, E., Bogush, A., Schlumberger, S., Weibel, G., Braga, R., Funari, V., Hyks, J., Rasmussen, E., Lederer, J., 2018. Technologies for the management of MSW incineration ashes from gas cleaning: new perspectives on recovery of secondary raw materials and circular economy. Sci. Total Environ. 635, 526–542. https://doi.org/10.1016/j.scitotenv.2018.04.150.

Rachwał, M., Kardel, K., Magiera, T., Bens, O., 2017. Application of magnetic susceptibility in assessment of heavy metal contamination of Saxonian soil (Germany) caused by industrial dust deposition. Geoderma 295, 10–21. https://doi.org/10.1016/j.geoderma.2017.02.007.

Reyes, B.A., Bautista, F., Goguitchaichvili, A., Morton, O., 2011. Magnetic monitoring of top soils of Merida (Southern Mexico). Studia Geophys. Geod. 55 (2), 377–388. https://doi.org/10.1007/s11200-011-0021-6.

Song, Y., Ji, J., Yang, Z., Yuan, X., Mao, C., Frost, R.L., Ayoko, G.A., 2011. Geochemical behavior assessment and apportionment of heavy metal contaminants in the bottom sediments of lower reach of Changjiang River. Catena 85, 73–81.

Szuszkiewicz, M., Magiera, T., Kapička, A., Petrovský, E., Grison, H., Gołuchowska, B., 2015. Magnetic characteristics of industrial dust from different sources of emission: a case study of Poland. J. Appl. Geophys. 116, 84–92. https://doi.org/10.1016/j.jappgeo.2015.02.027.

Thompson, R., Oldfield, F., 1986. Environmental Magnetism, 1 ed. Springer Netherlands, London, p. 228. https://doi.org/10.1007/978-94-011-8036-8.

Vigliotti, L., Capotondi, L., Torii, M., 1999. Magnetic properties of sediments

deposited in suboxic-anoxic environments: relationships with biological and geochemical proxies. Geol. Soc. Lond. Spec. Publ. 151 (1), 71–83. https://doi.org/10.1144/gsl.sp.1999.151.01.08.

Wang, X., Løvlie, R., Zhao, X., Yang, Z., Jiang, F., Wang, S., 2010. Quantifying ultrafine pedogenic magnetic particles in Chinese loess by monitoring viscous decay of superparamagnetism. G-cubed 11 (10). https://doi.org/10.1029/2010gc003194 n/a-n/a.

Wang, G., Deng, J., Ma, Z., Hao, J., Jiang, J., 2018. Characteristics of filterable and condensable particulate matter emitted from two waste incineration power plants in China. Sci. Total Environ. 639, 695–704. https://doi.org/10.1016/j.scitotenv.2018.05.105.

Yang, T., Liu, Q., Chan, L., Cao, G., 2007. Magnetic investigation of heavy metals contamination in urban topsoils around the East Lake, Wuhan, China. Geophys. J. Int. 171 (2), 603–612. https://doi.org/10.1111/j.1365-246X.2007.03558.x.

Zhang, C., Qiao, Q., Piper, J.D., Huang, B., 2011. Assessment of heavy metal pollution from a Fe-smelting plant in urban river sediments using environmental magnetic and geochemical methods. Environ. Pollut. 159 (10), 3057–3070. https://doi.org/10.1016/j.envpol.2011.04.006.

Zhu, Z., Li, Z., Bi, X., Han, Z., Yu, G., 2013. Response of magnetic properties to heavy metal pollution in dust from three industrial cities in China. J. Hazard Mater. 246–247, 189–198. https://doi.org/10.1016/j.jhazmat.2012.12.024.